Optimal design of multi-nozzle etching process for shadow mask

Minkyo Seo*, Jin Soo Park*, Sangdae Park**, and Jae Hak Jung*,†

*School of Display and Chemical Engineering, Yeungnam University,
214-1, Dae-dong, Gyeongsan, Gyeongbuk, Korea
**Samsung Everland Inc., 87 Euljiro 1ga, Jung-gu, Seoul, Korea

Abstract−This paper presents a new design approach of a multi-nozzle etching process which is the core system for the production of a shadow mask. The shadow mask, which is a thin metal plate with a huge number of small holes in regular patterns, is a key component of televisions and computer monitors. The shadow mask plays an important role in controlling the definition, color and distinction of televisions and computer monitors. Thus, the development of a rigorous and systematic design method for a multi-nozzle etching process to manufacture the shadow mask is beneficial particularly from the viewpoint of increasing efficiency and improving productivity. The proposed design method is based on simulating the complex spraying pattern using a Monte-Carlo method, whereas a stochastic method, so-called genetic algorithm, is used for an optimization tool. In such a highly complex solution space, the genetic algorithm searches optimal solutions efficiently and effectively. The simulation of spraying pattern for the multi-nozzle system and the genetic algorithm are coded by C language, while the graphic representations are attained by MATLAB graphic tools.

Key words: Multi-nozzle, Etching Process, GA, MATLAB

INTRODUCTION

For the last three decades, many shadow masks have been consumed in television manufacturing and for the production of computer monitors. The most common way of shadow mask manufacturing is to utilize a multi-nozzle etching process. Recently, large sizes of shadow masks are increasingly required as customers prefer larger televisions and computer monitors. To deal with the demand flexibly and effectively, a systematic design tool for the multi-nozzle etching process to produce shadow mask is even more needed.

The multi-nozzle etching process considered in this study is the system for the production of shadow mask. Here, the shadow mask is a perforated metal sheet inside a television and a color monitor. Most color monitor screens use cathode-ray tube (CRT) technology in which electrons are fired from an electron gun onto a fluorescent plate. The phosphor converts the kinetic energy of the electrons into light and is illuminated in small red, green and blue dots. Before the electron beam reaches the phosphor dots, it passes through shadow mask and the shadow mask ensures that the electron beam hits only the correctly colored phosphor dots and does not illuminate more than one dot. In addition, the shadow mask absorbs electrons that are directed at the wrong color phosphor, guiding the electron beams from the electron gun in the right direction. For the shadow mask, a variety of researches have been performed and can be readily found [1-3]. However, it is worth mentioning that the previous researches focused on the etching process and the raw materials rather than the multi-nozzle process.

The nozzle considered in this study is a spray nozzle which has been applied in a variety of areas such as coating, etching, cooling

processes, pollution control, etc. [4-7]. In general, a spray is the break-up of a volume of liquid into droplets (mist), i.e., atomization of liquid. The droplets (mist) are produced when a liquid enters the thin channel of nozzle. Of course, the size of the cone angle and the uniformity of droplets are highly dependent upon the pressure, the flow rate of a solution, the size of holes, and so forth. Finally, this spray occurs in a single nozzle, and these single nozzles are the elements of a multi-nozzle process.

Although the multi-nozzle etching process is commonly used to produce the shadow masks, there has been little attention for the design of the multi-nozzle process. It is purely because of a large number of parameters to be handled and their complex interrelationships. Fig. 1 shows the multi-nozzle etching process considered
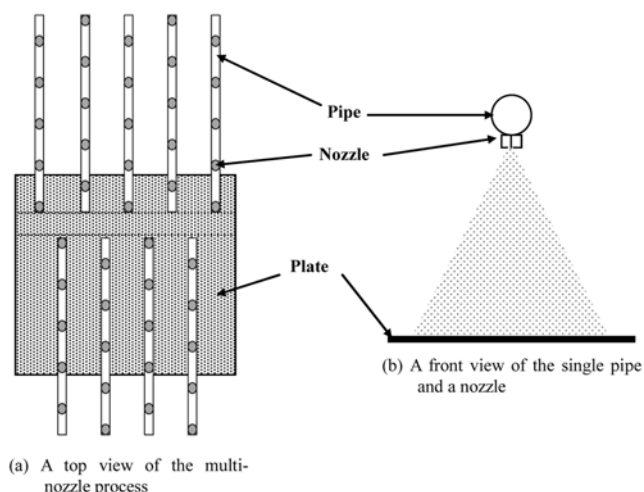

(a) A top view of the multi-nozzle process

(b) A front view of the single pipe and a nozzle

Fig. 1. The process diagram of the multi-nozzle system.

†To whom correspondence should be addressed.
E-mail: jhjung@ynu.ac.kr

in this study. Fig. 1(a) depicts the top view of the arrangements of pipes and nozzles, while its front view is shown in Fig. 1(b). As seen in Fig. 1, various parameters which affect the quality of shadow mask can be found, such as the distance between pipes, interval of nozzles, distance between a nozzle and the plate, etc.
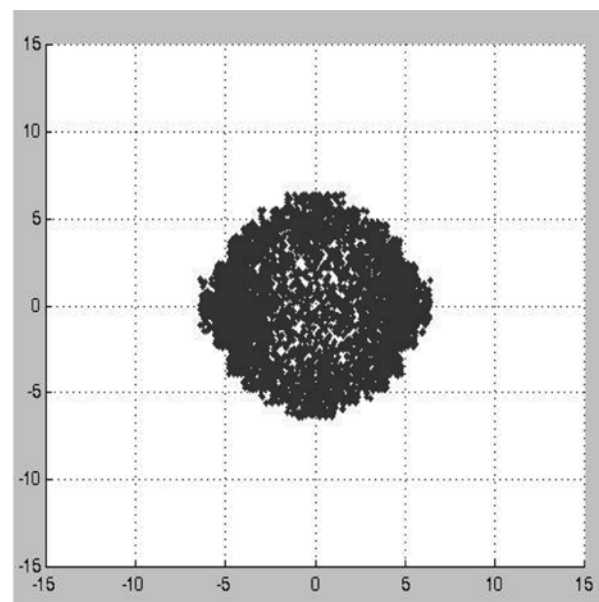
In general, the objective of the multi-nozzle etching process is to get a uniform etching quality of the surface on the moving plate with the least surface roughness on the moving plate by spraying the etching liquid equally all over the plate. To tackle this complex optimization problem, a rigorous simulation model for a spray nozzle was firstly developed by using the Monte-Carlo approach. Then, the complex design problem with a number of design variables was handled by genetic algorithm (GA). The genetic algorithm was based on natural selection and mechanics of nature and developed for the purpose of modeling the adaptation and evolution of nature [8-12]. The genetic algorithm is also able to decrease the probability of searching the wrong peak in multi-modal search spaces because it has the characteristic of parallel search. Therefore, the genetic algorithm has a wide acceptance as an efficient and robust search method because it increases the search speed for optimal solution and helps to escape from a local optimum in complex search spaces [13-18]. In this study, the simulation model for the spray nozzle and genetic algorithm were coded by C programming language. However, MATLAB was used for the visual representation of the simulation results. All computational results were obtained from an IBM-PC, 1.5 GHz CPU with 512 MB memory. Finally, the optimal design values were successfully obtained by the proposed method, and the GA showed a superior performance in search speed and efficiency.

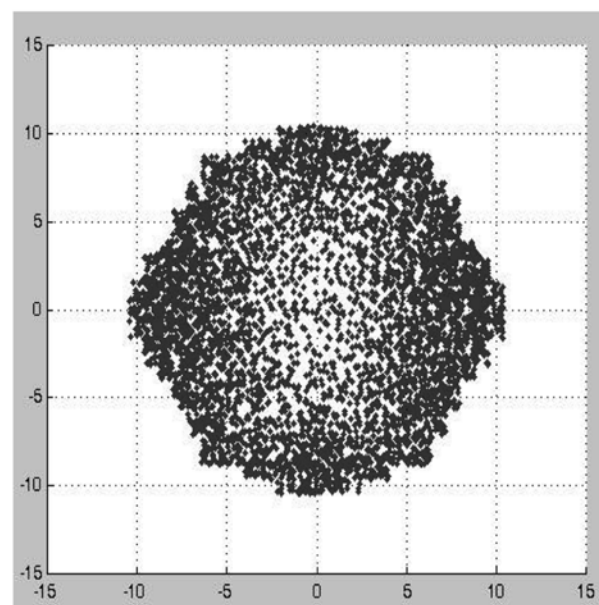## MODELING OF MULTI-NOZZLE ETCHING PROCESS

As mentioned earlier, the multi-nozzle etching process considered in this study is for the production of the shadow mask which is the key element of televisions and computer monitors. As the raw materials of the shadow mask, both aluminum-killed steel and invar alloy steel are commonly used for the shadow mask manufacturing. Although aluminum-killed steel plate has uniform etching and forming features, the invar alloy (64% Fe - 36% Ni) with the low thermal expanding feature is more commonly used. On the other hand, the ferric chloride solution ($FeCl_3$) as the etching liquid is sprayed from the nozzles onto the plate. As a result, the chemical etching of the plate is complete. The particular features in the multi-nozzle etching process are i) that the plate is moving at a given speed by a conveyer, and ii) that the pipes with nozzles are oscillating within an angle generated by the 4-bar crank-rocker mechanism (see the Appendix). In this study, the spray processing of the single nozzle was firstly analyzed, and then the modeling and simulation of the multi-nozzle etching process is explained in detail.

1. Analysis for Single Nozzle System

In this study, simulation for the spray processing of single nozzle is carried out on the basis of the experiment data. For the sampling of a liquid distribution, a 150 cm×150 cm plate was divided into equal-sized cells of 1 cm×1 cm. Then all of the cells were individually measured after spraying a liquid. In this case water was used as the spray liquid for the sampling. As a result, the experimental distribution data could be attained. Based on the volumetric distri-

(a) Distribution when the distance is 10 cm

(b) Distribution when the distance is 20 cm

Fig. 2. Distribution of droplets according to the distance.

bution data, 30,000 random numbers were generated for one spray.

Fig. 2 shows the simulation result of the spray depending on the distance between the nozzle and the plate. As expected, a wider distribution is obtained when the distance is farther. Another aspect to be accurately analyzed is the effect from the fact that the plate is moving with a given speed and the pipe is regularly oscillating within a given angle. A coordinate change of a droplet by the pipe's oscillation and the plate's movement is analyzed geometrically as shown in Fig. 3. As explained in the Appendix, the oscillating angle γ given by crank-rocker mechanism is the same as the angle of the nozzle measured from downward vertical.

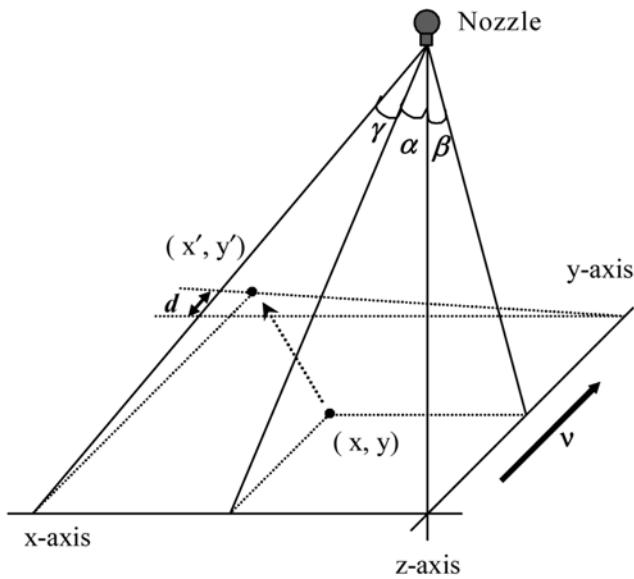Let us consider the coordinates (x, y) of an arbitrary droplet from

Fig. 3. **Graphical representations for the coordinate change of a droplet.**

a nozzle. When the pipe is oscillated by γ and the plate moves forward by d, new coordinates (x', y') can be presented as below in Eq. (1).

$$x' = L \cdot \tan(\alpha + \gamma)$$
$$y' = \frac{L \cdot \tan(\beta)}{\cos(\alpha + \gamma)} + d \qquad (1)$$

In Eq. (1), L indicates the perpendicular distance between a nozzle and the plate. And the two angles α and β can be obtained by Eq. (2).

$$\alpha = \tan^{-1}(x/L)$$
$$\beta = \tan^{-1}(y/L) \qquad (2)$$

As explained in the Appendix, the oscillating angle γ can be estimated by Eq. (A6). Eq. (3) below shows the relationship between the distance d and the rotating angle θ. In the equation, v is a constant linear velocity of the plate, while ω is an angular velocity of the shortest link AB in Fig. A1. In particular, the numerator v/ω means the moving interval per one rotation of the link AB.

$$d = \frac{v/\omega}{2\pi} \cdot \theta, \quad \theta \leq \theta \leq 2\pi \qquad (3)$$

Consequently, new coordinates (x', y') can be estimated by Eqs. (1), (2) (3) and (A6). Although the nozzle system is operating continuously, i.e., droplets are sprayed continuously from the nozzles, it is not straightforward to simulate this system as it stands. For this reason, the spray operation is considered and simulated as a discrete operation. Moreover, it is more beneficial to use discrete functions in the simulation from the viewpoint of the computational times. In this study, the rotating angle θ is divided into an equal-sized angle as shown in Eq. (4). And, the number of discretizations considered is 20 (N=20), which are obtained by heuristically. Lastly, Eqs. (5) and (6), which are correspondent with Eqs. (2) and (A6), respectively, are used in the simulation.

$$\theta_i = \frac{2\pi}{N} \cdot i, \quad i = \{0, 1, \dots, N-1, N\} \qquad (4)$$
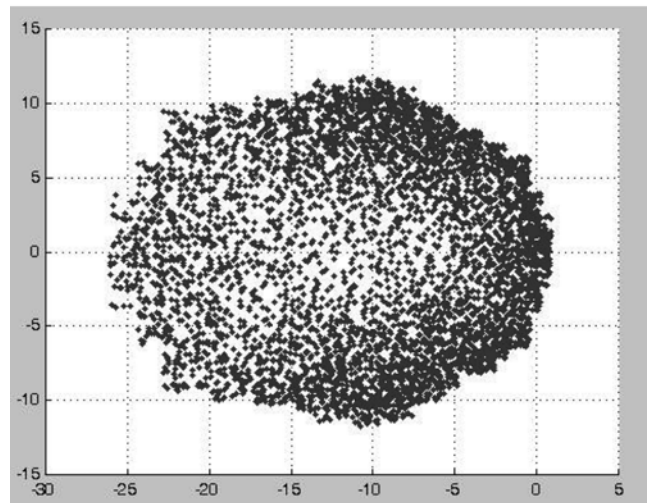
$$d_i = \frac{v/\omega}{2\pi} \cdot \theta_i \qquad (5)$$

$$\gamma_1 = \cos^{-1}\left(\frac{2\overline{AD}^2 - 2\overline{AD}\,\overline{AB}\cos\theta_i}{2\overline{AD}\sqrt{\overline{AD}^2 + \overline{AB}^2 - 2\overline{AD}\,\overline{AB}\cos\theta_i}}\right)$$

$$\gamma_2 = \cos^{-1}\left(\frac{\overline{CD}^2 + \overline{AD}^2 + \overline{AB}^2 - \overline{BC}^2 - 2\overline{AD}\,\overline{AB}\cos\theta_i}{2\overline{CD}\sqrt{\overline{AD}^2 + \overline{AB}^2 - 2\overline{AD}\,\overline{AB}\cos\theta_i}}\right) \qquad (6)$$

$$\gamma_i = \begin{cases} \gamma_2 + \gamma_1, & 0 \leq \theta \leq \pi \\ \gamma_2 - \gamma_1, & \pi \leq \theta \leq 2\pi \end{cases}$$

A new distribution of droplets caused by the changes of an oscillating angle is illustrated in Fig. 4. As seen in Fig. 4(b), the distribution that an oscillating angle is $-25°$ becomes clearly asymmetrical, and the distribution area is bigger and wider.

(a) Distribution when the oscillating angle is zero

(b) Distribution when the oscillating angle is $-25°$

Fig. 4. **The Effects for the changes of the oscillating angle.**

2. Simulation of Multi-nozzle Process

In this study, a simulation of a multi-nozzle system is performed on the basis of a single nozzle simulation. All nozzles of which positions are distinguished by the arrangement of pipes and nozzles are simulated individually, but the simulation results are accumulated. Fig. 5 indicates the distribution results of one nozzle, while
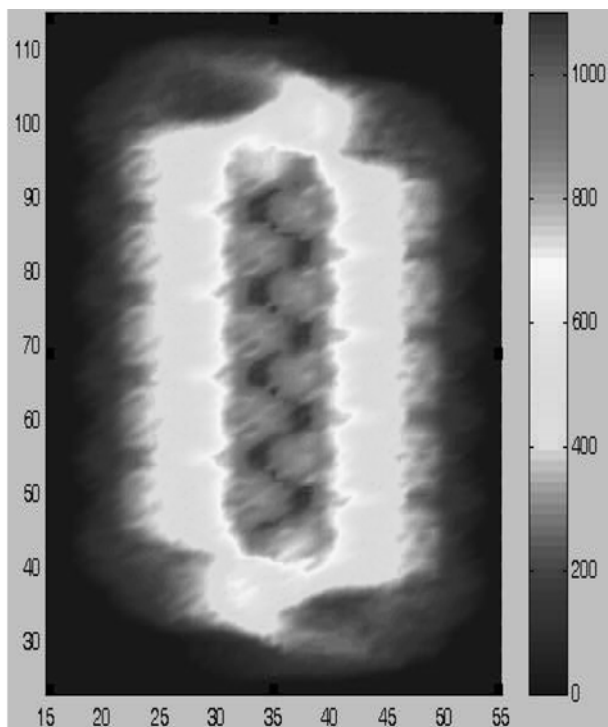

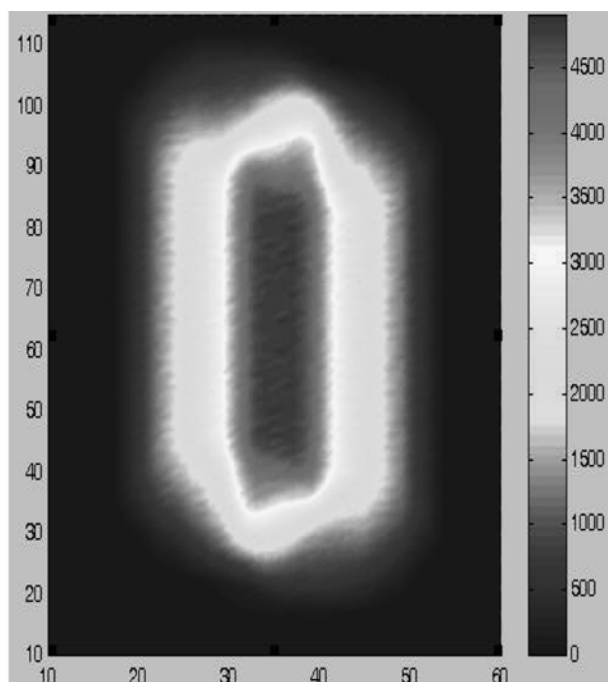Fig. 5. Distribution result by one nozzle.

Fig. 6. Distribution from five nozzles in one pipe.

Fig. 6 shows the cumulative distribution results from five nozzles in one pipe. The sinuous wave shown in Fig. 5 disappears in Fig. 6, i.e., the distribution of droplets from five nozzles is more uniform than that from a single nozzle. On the other hand, Fig. 7 shows two mountains of droplets in the middle as the result of ten nozzles within two neighboring pipes. This is the evidence why optimization is required for the multi-nozzle process in order to get the best uniformity of sprayed droplets. Figs. 5, 6 and 7 are the top views of the moving plates.

3. Design Variables

The whole structure of the multi-nozzle etching process is composed of five pipes in which five nozzles are arranged. In this study, the major factors affecting the performance of the multi-nozzle system are classified into two categories. One is *structure variables* concerning the layouts of multi-nozzle etching process, i.e., the pipe pitch (Pp), the nozzle pitch (Np) and the perpendicular distance between a nozzle and the plate (L). The other is *operation variables* regarding the processing of that system after the layout is determined. The operation variables considered in this work are the total oscillating angle (Γ), the angular velocity of the shortest link AB

Fig. 7. Distribution from nozzles in two adjacent pipes.

Table 1. Bounds of design variables

Variables		Lower bound	Upper bound
Name	UNIT		
Pp	[cm]	10.0	25.0
Np	[cm]	15.0	30.0
L	[cm]	10.0	20.0
Γ	[degree]	30.0	61.0
ω	[rpm]	30.0	61.0
ν	[cm/min]	300.0	610.0

in the crank-rocker mechanism (w) and the plate speed (v). Both the structure and the operation variables are illustrated in Figs. 8 and 9, while Table 1 shows the lower and upper bounds of the variables taken into account in this study. However, it is assumed that pipes and nozzles are regularly arranged, so that all the intervals of the neighboring nozzles are equivalent as Np, and the distances of the adjacent pipes are the same as Pp.

GENETIC ALGORITHM

The genetic algorithm (GA), which is based on natural selection and the mechanics of natural genetics, was introduced by J. Holland (1975) and has been developed for the purpose of modeling the adaptation and evolution of nature [8]. GA decreases the probability to search a wrong peak by carrying out a parallel search in order to exploit a population of peaks in multi-modal search space. GA is an efficient and robust search method because it increases the search speed for optimal solution and helps to escape from a local optimum in complex search spaces.

Compared with the conventional optimization method, GA has several characteristics. First, GA searches the solution not using the parameters per se but using parameter coding. GA uses only the function value regardless of how to proceed inside the parameter set. Among many individuals, GA selects more suitable parameter values for the given objective function using a relevant probability transition rule and efficiently increases the number of superior elements. As GA exploits the solution using parameter coding, it is

little influenced by the restrictions such as continuity of function, existence of derivative, convexity, etc. Second, GA searches the solution by using many points, not a single point. Other optimization methods search from one position to another position using a specific transition rule such as negative gradient direction. These methods are greatly affected by the position of the initial solution, while GA has a high probability to reach a global optimum compared to the conventional methods by using the coding of many parameters to search the optimal solution. Third, as GA uses only the function value, there is no need to consider auxiliary knowledge such as derivatives, continuity, and so forth. Fourth, GA uses probabilistic transition rules, not deterministic rules. In other words, GA uses probabilistic transition rules. Probabilistic transition rules use random choice in order to find the optimal solution in the search space. This means the evolution by random selection, not a simple random search method.

The reason GA is adapted to a variety of areas is that it has robustness presenting the balance between efficiency and efficacy for searching the solution. When the circumstance of the given problem variables, this robustness decreases the necessity of redesign by the alteration of control parameters of GA.

1. Basic Operators

The reproduction operator, i.e., an artificial version of natural selection, selects elements from the parent generation by the rule named the survival of the fittest in order to reproduce new individuals. Reproduction operation is processed by stochastic remainder selection without replacement proposed by De Jong [19]. This means that the same number as the integer number of the expected value is copied into the mating pool and the real number of the expected value is processed by flip function with weight. In the case of using a traditional selection rule, several elements with abnormal fitness severely affect one generation. This may bring about premature convergence. So, it is very important to adjust for the fitness of parent individuals in this operator. For this reason, GA requires the fitness scaling discriminating individuals with similar fitness. Even if linear scaling is generally used in most genetic algorithms, it has a trouble that scaled individuals with negative fitness value appear in the next generation when the minimum number of inferior individuals is much smaller than that of average fitness of the generation. To overcome this trouble of linear scaling, the sigmoid scaling function shown in Eq. (7) was used in this work.
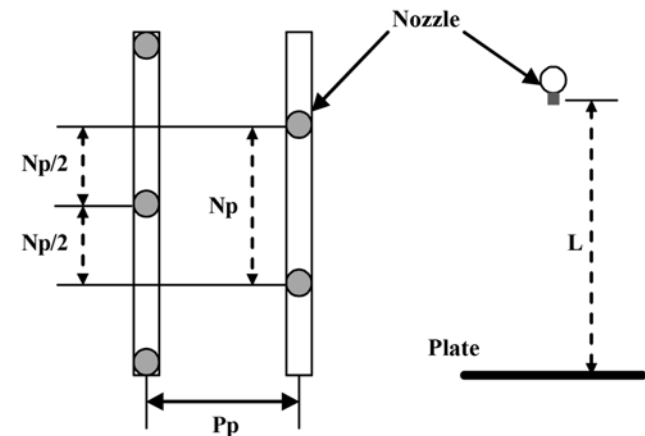
$$f' = \frac{2}{1 + \exp(-\lambda x)} \tag{7}$$
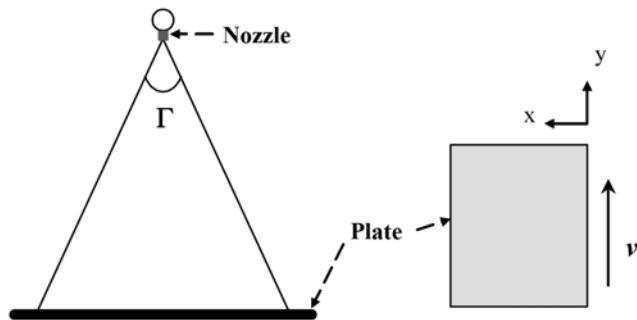

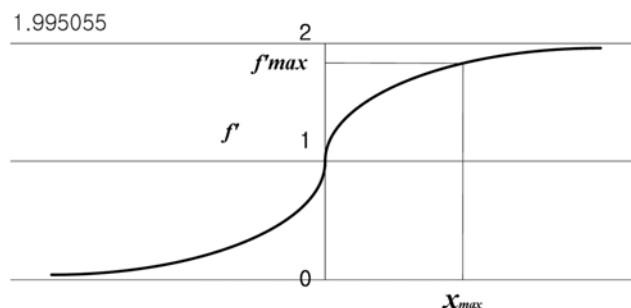Fig. 8. The structure variables.

Fig. 9. The operation variables.

Fig. 10. Sigmoid scaling function used in fitness scaling.

to produce individuals of the next generation. Therefore, G has a value between 0 and 1. If G is 1, then this means non-overlapping population; if G is not 1, in means overlapping population. For most optimization problems, it was said that the non-overlapping population model was superior to the overlapping population model.

3. Computational Results

Table 2 shows the result of genetic algorithm where the advanced operators (N=40, Gen=10, Pc=1.0, Pm=0.1 and G=1) were used. Best cases were presented in Figs. 13 and 14. The worst cases were

Table 2. The result of genetic algorithm

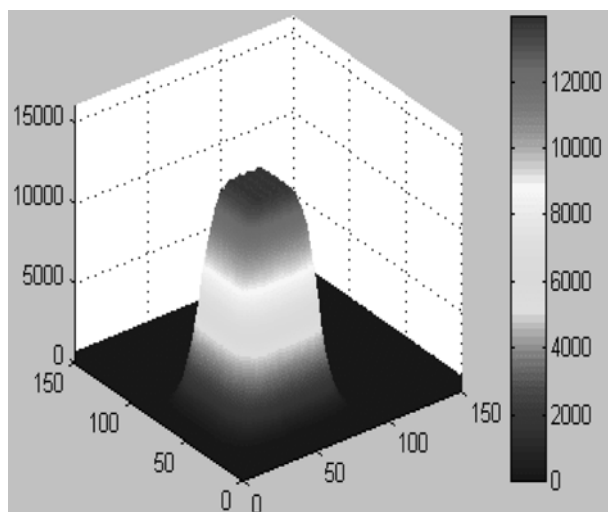|	L	P_p	N_p	Θ	ω	ν	$\sigma(\times 10^5)$
GOOD	15.5	12	17	39	51	3.1	1.78
	15.5	12	25	40	52	3.1	1.95
	15.5	12	25	39	53	3.1	1.98
BAD	17	25	20	48	59	3.8	96.83
	17	25	15	53	35	3.6	99.77
	15	25	26	37	32	3.1	115.04

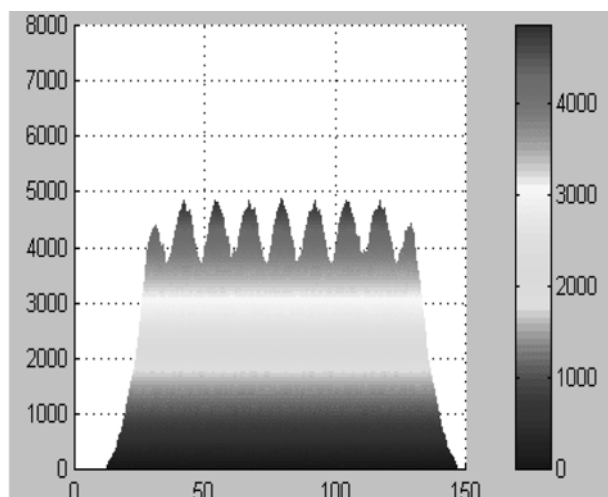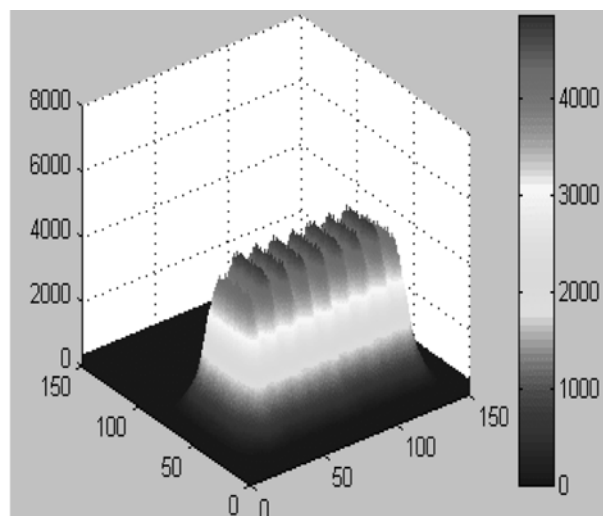**Fig. 14. Best case (2).**

Fig. 15. Worst case (1).

Fig. 16. Worst case (2).

represented Figs. 15 and 16. From the result of GA, it is shown that good solutions are located in solution space where the plate speed is slow and angular velocity is fast.

CONCLUSION

A step change test of heater level and pull speed were performed at various points in this study; genetic algorithm was programmed by C Language and applied to process modeling.

Even though the target process in this study is designed in detail, it is better to find the region of good solution than to find down to the last decimals of each variable if we are considering that some disturbances and vibrations can occur in the multi-nozzle etching process.

So now, we have come to the conclusion that its tendency is similar to the target line by the result of programming and, on the basis of the result, we can simulate the process while changing various parameters.

ACKNOWLEDGMENT

REFERENCES

1. R. B. Maynard, J. J. Moscony and M. H. Saunders, *Ferric chloride etching of low carbon steels*, RCA Rev., **45**, 73 (1984).
2. R. B. Maynard, J. J. Moscony and M. H. Saunders, *Ferric chloride etching of Invar*, RCA Rev., **47**, 88 (1986).
3. G. J. Kwon, H. Y. Sun and H. J. Sohn, *J. Electrochem. Soc.*, **142**, 3016 (1995).
4. M. Hariki, A. Nishi and M. Morita, *Tetsu-to-hagané.*, **83**, 257 (1997).
5. G. E. Mccreery and C. M. Stoots, *Int. J. Multiphase Flow*, **22**, 431 (1996).
6. M. Sommerfield and H. H. Qiu, *Int. J. Heat Fluid Fl.*, **19**, 10 (1998).
7. M. V. Panchagnula and P. E. Sojka, *Fuel*, **78**, 729 (1999).
8. J. H. Holland, *Adaptation in natural and artificial systems*, Univer-

sity of Michigan Press, MI (1975).

9. D. E. Goldberg and R. Lingle, *Proceedings of the International Conference on Genetic Algorithms and Their Applications*, 154 (1985).

10. D. E. Goldberg, *Engineering with Computers*, **3**, 35 (1987).

11. D. E. Goldberg, *Genetic algorithms in search, optimization and machine learning*, Addison-Wesley Publishing Co. (1989).

12. G. J. E. Rawlins, *Foundation of genetic algorithms*, Morgan Kanfmann Publishers, San Mateo (1991).

13. L. Davis, *Genetic algorithms and simulated annealing*, Morgan Kanfmann Publishers, San Mateo (1987).

14. J. H. Jung, C. H. Lee and I. B. Lee, *Comput. Chem. Eng.*, **22**, 1725 (1998).

15. L. Davis, *Handbook of genetic algorithms*, Van Nostrand ReinHold, New York (1991).

16. Y. Davidor, *Genetic algorithms and robotics: A heuristic strategy for optimization*, World Scientific, Singapore (1991).

17. S. Park, H. Cho, H. Lee and L. Jeon, *'92 KACC (Domestic) at Seoul*, 863 (1992).

18. Y. Kim, H. Kang and H. Jeon, *'92 KACC (Domestic) at Seoul*, 698 (1992).

19. K. A. De Jong, *Proceedings of the International Conference on Genetic Algorithms and Their Application*, 210 (1995).

APPENDIX I. FOUR-BAR CRANK-ROCKER MECHANISM

Fig. A1 shows the 4-bar crank-rocker mechanism. The link AD is fixed in the crank-rocker system, while the link BC is a connecting link. In fact, the shortest link AB can make a full revolution, which affects the oscillation of the opposite link CD. Namely, the link CD rocks as the link AB revolves. As illustrated in Fig. A1, the oscillating angle γ is measured as $\angle ADC$ and has two limits, γ_{min} and γ_{max}, i.e., $\gamma_{min} \leq \gamma \leq \gamma_{max}$. The difference between two limits, $\Gamma = \gamma_{max} - \gamma_{min}$ is the magnitude of the oscillating angle generated by the rotation of the link AB.

In this study, the total oscillating angle G means the spray angle of nozzles. In addition, G is one of the most important variables which can affect the performance of the etching process. In the event that the links BC, CD and DA are predetermined, the total oscillating angle Γ simply becomes a function of the link AB. Let us consider two triangles ΔC_1DA and ΔC_2DA in order to demonstrate the relationship between Γ and the length of AB. In ΔC_1DA, γ_{max} can be written as below according to the law of cosines,

$$\gamma_{max} = \cos^{-1}\left(\frac{\overline{AD}^2 + \overline{C_1D}^2 - \overline{C_1A}^2}{2\,\overline{AD}\,\overline{C_1D}}\right)$$

$$= \cos^{-1}\left(\frac{\overline{AD}^2 + \overline{CD}^2 - (\overline{BC} + \overline{AB})^2}{2\,\overline{AD}\,\overline{CD}}\right) \tag{A1}$$

Similarly, γ_{min} can also be obtained from the cosine rule for ΔC_2DA:

$$\gamma_{min} = \cos^{-1}\left(\frac{\overline{AD}^2 + \overline{C_2D}^2 - \overline{C_2A}^2}{2\,\overline{AD}\,\overline{C_2D}}\right)$$

$$= \cos^{-1}\left(\frac{\overline{AD}^2 + \overline{CD}^2 - (\overline{BC} + \overline{AB})^2}{2\,\overline{AD}\,\overline{CD}}\right) \tag{A2}$$

Therefore, Γ is simply presented as a function of the length of AB under the assumption that the links BC, CD and DA are fixed, which is shown in Eq. (A3). Consequently, the total oscillating angle can be estimated as the length of AB is given, and vice versa.

$$\Gamma = \cos^{-1}\left(\frac{\overline{AD}^2 + \overline{CD}^2 - (\overline{BC} + \overline{AB})^2}{2\,\overline{AD}\,\overline{CD}}\right)$$

$$- \cos^{-1}\left(\frac{\overline{AD}^2 + \overline{CD}^2 - (\overline{BC} + \overline{AB})^2}{2\,\overline{AD}\,\overline{CD}}\right) \tag{A3}$$

Another important factor to be considered is the relationship between the oscillating angle γ and the rotating angle θ.

Let us consider two triangles ΔDAB and ΔCDB as shown in Fig. A2. In this case, the imaginary line BD is drawn for the sake of the analysis. For the triangle ΔDAB, the cosine rule for the angle θ can be written as Eq. (A4). On the other hand, Eq. (A5) is obtained from the cosine rules against the angles γ_1 and γ_2. Finally, the oscillating angle γ, $\angle ADC$ is determined by Eq. (A6) as below.

$$\overline{BD} = \sqrt{\overline{AD}^2 + \overline{AB}^2 - 2\,\overline{AD}\,\overline{AB}\cos\theta}, \quad 0 \leq \theta \leq 2\pi \tag{A4}$$

$$\gamma_1 = \cos^{-1}\left(\frac{\overline{AD}^2 + \overline{BD}^2 - \overline{AB}^2}{2\,\overline{AD}\,\overline{BD}}\right)$$

$$\gamma_2 = \cos^{-1}\left(\frac{\overline{CD}^2 + \overline{BD}^2 - \overline{BC}^2}{2\,\overline{CD}\,\overline{BD}}\right) \tag{A5}$$

$$\gamma = \begin{cases} \gamma_2 + \gamma_1, & 0 \leq \theta \leq \pi \\ \gamma_2 - \gamma_1, & \pi \leq \theta \leq 2\pi \end{cases} \tag{A6}$$
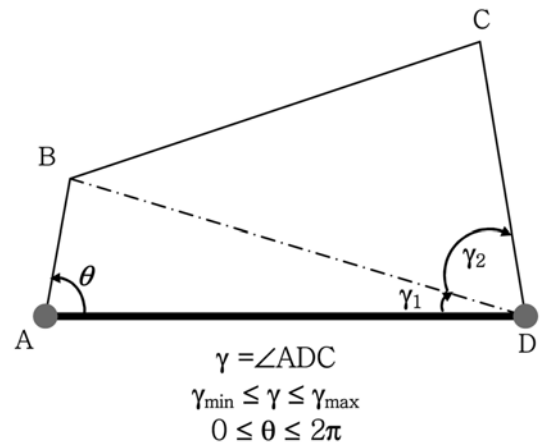

Fig. A1. The 4-bar crank-rocker mechanism.
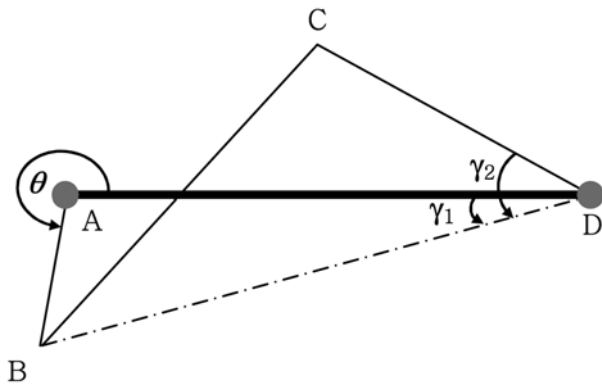

Fig. A2. An example of 4 bar linkages.

Fig. A3. The changes of γ_1 and γ_2 when $\theta \geq 180°$.

Fig. A4. The relationship between γ and θ.

Fig. A3 depicts the angles γ_1 and γ_2 when the rotation angle θ is greater than 180°. Thus, the angle γ, $\angle ADC$ is determined as $\gamma = \gamma_2 - \gamma_1$.

From the relationship shown in Eq. (A6), the change of the oscil-
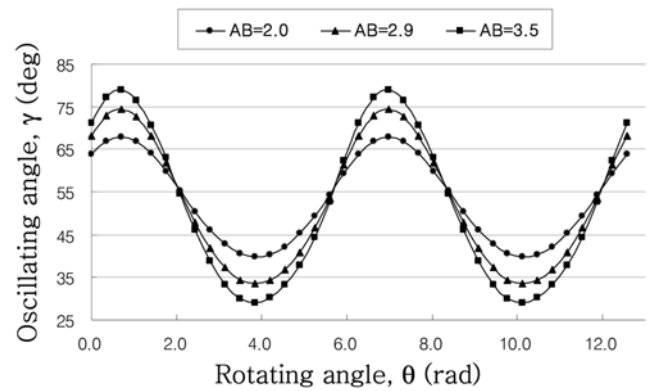
lating angle γ versus a change of θ can be estimated. Fig. A4 shows the relationship between γ and θ depending on the length of AB. The frequency is similar regardless of the length of AB, whereas the amplitudes are increased proportionally with the length of AB.